PASJ: Publ. Astron. Soc. Japan **47**, 251–263 (1995)

Energetics and Occurrence Rate of Active-Region Transient Brightenings and Implications for the Heating of the Active-Region Corona

Toshifumi SHIMIZU
Institute of Astronomy, The University of Tokyo, Mitaka, Tokyo 181

(Received 1994 November 15; accepted 1995 January 12)

Abstract

Frequent transient brightenings have been discovered in solar active regions using the Yohkoh Soft X-ray Telescope. We examine the possibility that these transient brightenings have much contribution to heating of the active-region corona. Imaging observations provide the following physical conditions: temperature, 4–8 MK; emission measure, $10^{44.5}$–$10^{47.5}$ cm^{-3}; electron density, 2×10^9–2×10^{10} cm^{-3}; gas pressure, 5–20 dyne cm^{-2}; loop length, 5×10^3–4×10^4 km; loop width, 2×10^3–7×10^3 km; and duration, 2–7 min. The energy involved in the observed transient brightenings is estimated to range from 10^{25} to 10^{29} erg. The frequency distribution as a function of the energy can be represented by a single power-law with an index of 1.5–1.6 in the energy range greater than 10^{27} erg, although the distribution deviates from a power-law in the energy range less than 10^{27} erg due to the instrument dead time and/or obscuration by bright coronal features. The single power-law of the frequency distribution thus appears to extend from the solar flare range down to an energy of 10^{27} erg. The total energy supplied by transient brightenings and flares, assuming that the power-law continues to lower energy, is estimated to be at most a factor of 5 smaller than the heating rate required for the active-region corona. We need weaker events with an occurrence rate much higher than the extrapolated power-law to explain the heating of the active-region corona with transient brightenings.

Key words: Active regions — Coronal heating — Sun: activity — Sun: corona — Sun: X-rays

1. Introduction

The Soft X-ray Telescope (SXT, Tsuneta et al. 1991) aboard the Yohkoh satellite (Ogawara et al. 1991), launched on 1991 August 30, has revealed that active regions commonly have numerous flare-like loop brightenings (Shimizu et al. 1992, 1994). Intense transient brightenings have been identified as small soft X-ray enhancements in the GOES time profiles; also, SXT has observed fainter transient brightenings, which are not detectable in the GOES data (Shimizu et al. 1992). The quantitative relation of brighter transient brightenings with the corresponding enhancements in the GOES data is described in appendix 1. Tsuneta and Lemen (1993) have shown that the hard X-ray microflares observed by Lin et al. (1984) can be associated with small soft X-ray enhancements seen in the GOES time profiles, and suggested that intense transient brightenings observed by SXT are actually the soft X-ray counterparts of hard X-ray microflares.

Transient brightenings show great variety in X-ray morphology (Shimizu et al. 1994; Shimizu 1994). They are mostly in the form of multiple or single loops, although some brightenings are point-like. The loops tend to brighten from their footpoints and/or the sites where the loops are apparently in contact during the initial phase of the brightenings, followed by brightenings of the entire loops.

A new concept concerning heating of the corona arises from the finding of hard X-ray microflares using a balloon-borne hard X-ray detector (13–600 keV) with a very high sensitivity. Numerous microscopic energy releases (microflares or nanoflares) may be a possible source for heating the corona (Lin et al. 1984; Parker 1988). The frequency distribution of the energy releases as a function of the magnitude is, therefore, important information which can be used to examine the microflare heating hypothesis.

The frequency distribution of large energy releases (solar flares) has been established mainly by hard X-ray observations during the past 20 years. Solar flares have a single power-law frequency distribution. Datlowe, Elcan, and Hudson (1974) have shown that the integral distribution of the peak hard X-ray flux at 20 keV, observed by the Seventh Orbiting Solar Observatory (OSO 7), had a power-law dependence with an index of 0.8 : $N(> F_\mathrm{P}) \propto F_\mathrm{P}^{-0.8}$, where $N(> F_\mathrm{P})$ is the occurrence rate of flares with a peak flux greater than F_P. The differential distribution of hard X-ray flares measured by the Hard X-Ray Burst Spectrometer (HXRBS) aboard the Solar Maximum Mission (SMM) has been found to have a power-law with an index of $\alpha \approx 1.8$ (Dennis 1985),

$$dN/dF_p \propto F_p^{-\alpha}, \tag{1}$$

where F_p is the peak photon count rate (above 25 keV). The power-law distribution of solar flares is also found in the soft X-ray range (Drake 1971); the power-law index is 1.75 for the peak flux at 2–12 Å and 1.44 for the time-integrated flux, $\int F dt$, where F is the soft X-ray flux. While these studies present only the distributions of the peak flux of solar flares at a specific wavelength, Crosby, Aschwanden, and Dennis (1992) have estimated the distribution of the time-integrated total nonthermal energy, assuming that solar-flare hard X-rays are produced by bremsstrahlung from a distribution of accelerated electrons impinging upon a thick target plasma. The distribution of the total nonthermal energy is represented by a power-law function over an energy range of 5×10^{28} to 10^{30} erg with a power-law index of 1.52.

Lin et al.'s observation of hard X-ray microflares shows that the integral distribution of microflares can be represented by a power-law function, down to the limit of the measurement, with a slope of about 1; the power-law index should be about 2 in the differential distribution. This power-law index is apparently larger than that of the larger events.

To discuss whether or not microflares are energetically more important than solar flares to heat the corona, we must study the distribution of the total energy released by microflares smaller than the events observed so far. If the occurrence rate per energy is a power-law function, i.e., $dN/dE = AE^{-\alpha}$, the total energy P in the distribution can be represented as

$$P = \int_{E_{\min}}^{E_{\max}} (dN/dE) E dE = \frac{A}{-\alpha+2} E^{-\alpha+2}\Big|_{E_{\min}}^{E_{\max}}, \tag{2}$$

where A and α are assumed to be constant. From this equation, $\alpha > 2$ implies that microflares are able to contribute to heating of the active-region corona, if $E_{\min}$ is sufficiently low, as suggested by Lin et al. (1984). Observations of solar flares have shown that the power-law index is less than 2; thus, flares in the ordinary range alone cannot heat active regions.

Since the transient brightenings observed by SXT are probably weaker events than Lin et al.'s hard X-ray microflares, we can therefore better examine the microflare heating hypothesis. The soft X-ray images give the soft X-ray intensity, source size, and duration of the transient brightenings. We can also determine the temperature and emission measure using broad-band filters (Vaiana et al. 1973; Hara et al. 1992; Kano, Tsuneta 1994). These physical parameters allow us to estimate the energy involved in the transient brightenings. In addition, we obtain the distribution functions of the occurrence rate of the transient brightenings. The distributions are obtained as a function of not only the soft X-ray peak intensity, but also the total energy, estimated using the observed physical parameters. In section 2 we describe our observation and the analysis methods. Some physical parameters concerning the transient brightenings are presented and compared with those of major flares in section 3. The distributions of the occurrence rate of the transient brightenings are shown in section 4. Using the frequency distribution obtained in section 4, the energy input by the sum of transient brightenings is estimated and compared with the heating rate required for the active-region corona in section 5. Finally, in section 6, we discuss the implications of our results for the heating of the active-region corona.

2. Observation and Analysis Methods

2.1. Observation

We used soft X-ray partial CCD images taken with SXT from 1992 August 15 to 20. During this period, the field of view of the partial images tracked an active region, NOAA 7260, which showed relatively high activity mainly on August 21 (Solar Geophysical Data). The field of view of the images is about $5' \times 5'$ and the pixel size is $2''\!.46$. The images were taken alternately through two different X-ray filters (Al 1265 Å and Al 12 μm filters) on a 64-s cycle. The observation at the high telemetry rate was limited to less than 50 min, because of a capacity limitation of the onboard data recorder and other interruptions. In this study we used sequences of images with a time coverage greater than 30 min at the high telemetry rate.

Active region NOAA 7260 had a well-developed large simple sunspot in the preceding area. Around this spot, satellite spots or moving magnetic features (Harvey, Harvey 1973) move outward in the radial direction. A continuous emergence of new magnetic flux was observed in the following plage area after August 15; it produced much activity, including M-class flares on August 20 and 21 (Leka et al. 1994). During the observation, more than 600 transient brightenings were observed in active region NOAA 7260. The appearance of the transient brightenings was mainly localized to two areas in the active region: one was around the outer boundary of the penumbra of the preceding spot; the other was the emerging flux region embedded in the following area (Shimizu 1993).

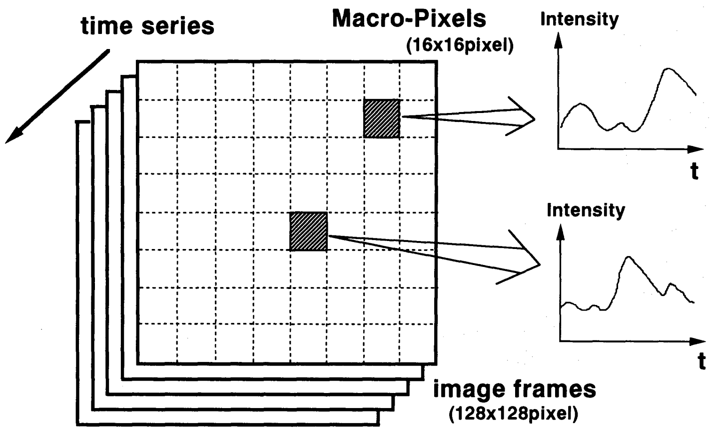

Fig. 1. Macro-pixel method: the soft X-ray image is divided into a "macro-pixel" image. Each macro-pixel has a light curve of the soft X-ray intensity. The enhancements in the light curve were systematically investigated.

2.2. Search for Transient Brightenings

In order to obtain distributions of the occurrence rate of transient brightenings, we need to identify transient brightenings which are as faint as possible. All of the features which showed small enhancements in the X-ray intensity in the sequence of soft X-ray images were thus accepted as being transient brightenings. Transient brightenings are identified using two independent methods: (1) by a visual inspection, and (2) by a "macro-pixel" method.

The first method, visual inspection, consists of identifying all features with small enhancements in intensity by visually inspecting the sequence of images. We then sum up the values of the CCD pixels covering the feature and obtain the time variations of the soft X-ray intensity. We identified 291 transient brightenings from the sequence of images (cumulative observing time 11.2 hr) in this way. This method may, however, miss faint transient brightenings which appear in the bright diffuse background of the active region.

We can systematically search for intensity enhancements by using light curves. It is clearly more difficult to find small transient enhancements from the light curves of the whole Sun or the wide field of view. We have therefore developed a "macro-pixel" method to make sure that the visual inspection method does not miss any faint transient brightenings. This method divides the original images (128×128 pixels) into macro-pixels, for example consisting of 16×16 pixels, and thus systematically pick up enhancements of the macro-pixel intensity using the light curve of each macro-pixel (figure 1). One transient brightening covers one, two, or more macro-pixels, which could affect the distribution function of the transient brightenings. This event-splitting effect is corrected: Enhancements extending over a few macro-pixels are assumed to result from one transient brightening when they are simultaneously observed. We searched for any intensity enhancements in the time profiles above the $3\,\sigma$ level of Poisson statistics of the incident photons.

We note that the following preparations were made before carrying out the above-mentioned analysis: data decompression, dark-current subtraction, satellite attitude jitter removal, and exposure-time normalization.

2.3. Determination of Physical Parameters

The light curves of transient brightenings give the soft X-ray peak intensity as well as the duration of transient brightenings for each X-ray filter, as illustrated in figure 2. The background intensity is taken to be the minimum intensity over a few minutes preceding a transient brightening (B_1, B_2, B_3). The peak intensity is defined as the maximum intensity in excess of the background (P_1–B_1, P_2–B_2, P_3–B_3). The light curves are spline-fitted so as to interpolate the data points (64 s interval) in order to estimate the soft X-ray peak intensity. This is important for obtaining accurate temperatures. The duration is defined as the duration for which the soft X-ray intensity exceeds half the peak intensity (E_1–S_1, E_2–S_2, E_3–S_3).

The soft X-ray images also give the sizes of the brightenings. Since many of the transient brightenings have clear loop-like structures (Shimizu et al. 1994), we determined the lengths and widths of the loops from the images. The plasma volume V is simply assumed to be lw^2, where l is the length and w is the width of the loop.

The temperatures and emission measures of the transient brightenings can be determined using the soft X-ray peak intensities obtained from the above-mentioned procedure. A combination of the peak intensities of Al 1265 Å and Al 12 μm filters is used to obtain the temperatures and emission measures with the assumption of

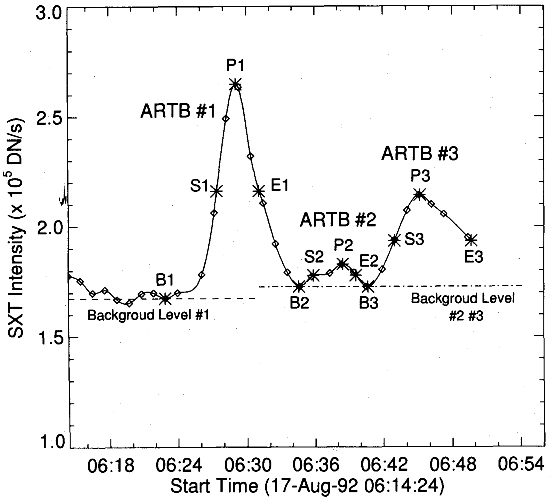

Fig. 2. Example of a soft X-ray light curve (Al 1265 Å filter) of a small area (27″ × 44″) in an active region. The diamonds are the observed intensities and a spline-fitting curve (the solid line) is used to interpolate them. Three transient brightenings were observed in the area during the period of 6:14–6:50 UT on 1992 August 17. The soft X-ray peak intensities of the transient brightenings are defined to be P_1–B_1, P_2–B_2, P_3–B_3. The durations are defined to be the period for which the soft X-ray intensity exceeds half of the peak intensity (E_1–S_1, E_2–S_2, E_3–S_3).

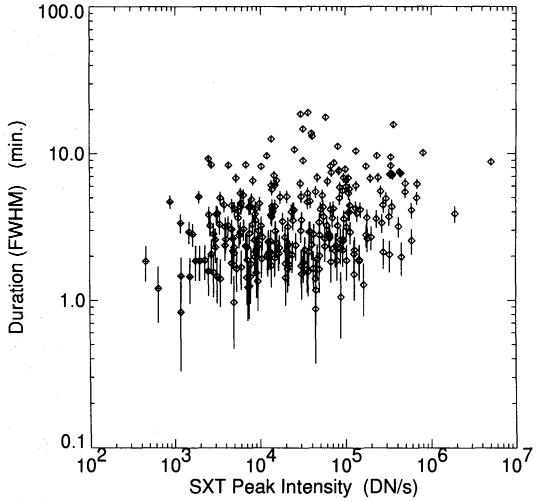

Fig. 3. Distribution of the duration of the transient brightenings as a function of the soft X-ray peak intensity through Al 1265 Å filter. The error bars on the duration represent half the time resolution (32 s), and those on the peak intensity represent ±1 σ uncertainties based on Poisson statistics of incident photons.

soft X-ray emission from isothermal plasma. Even if the plasma is multi-thermal, this combination gives a single temperature which is the weighted average of the differential distribution of the plasma temperatures with the filter transmission functions. This combination is suitable for determining the temperatures between 4–7 MK (Hara et al. 1992).

3. Physical Condition of Brightening Loops

The physical parameters of brightening loops are described in this section. The parameters derived directly from the data are the soft X-ray peak intensity, duration, loop size, temperature, and emission measure.

Figure 3 shows the distribution of the duration of transient brightenings as a function of the soft X-ray peak intensity through Al 1265 Å filter. The peak intensity is represented in units of DN s^{-1}. One DN (data number) corresponds to 100 electrons and to an energy of 5.8×10^{-10} erg at the SXT focal plane (Tsuneta et al. 1991). The error bars on the duration are estimated as half the time resolution (32 s), and those on the peak intensity represent ±1 σ uncertainties based on Poisson statistics of the incident photons.

Transient brightenings are widely distributed in the duration range from 1 to 20 min, most of which are concentrated in duration from 2 up to 7 min. Drake (1971) showed that the durations of major flares are 10–70 min in the soft X-ray range. The durations of transient brightenings are thus much shorter than those of the major flares. We note that transient brightenings with shorter duration (< 32 s) can exist, because the data used here have an ∼ 32 s dead time. Transient brightenings often exhibit a rapid rise with a longer-lived decay phase, as illustrated in figure 2. This behavior is also observed in major flares.

A power-law dependence was found for the frequency distribution of durations of major flares by Crosby, Aschwanden, and Dennis (1993) and Lee, Petrosian, and McTiernan (1993), whose results were based on hard X-ray observations. We also examined the frequency distribution of durations for the transient brightenings, and found a power-law dependence in the range of 2 to 20 min with an index of 2.5 (least-squares fitting), although the distribution deviates from the power-law in the range smaller than 2 min. This index is in good agreement with Crosby, Aschwanden, and Dennis's index 2.54 and Lee, Petrosian, and McTiernan's index 2.73, although they used different definitions of the duration.

The distribution of the loop sizes is presented in figures 4 (length) and 5 (width). Note that we assume that the errors in the length and width are ±1 CCD pixel

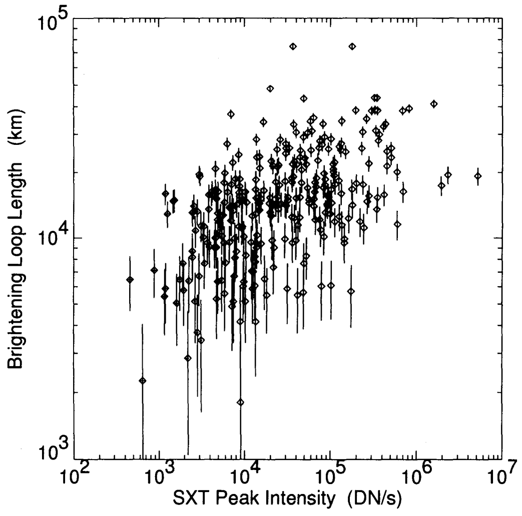

Fig. 4. Distribution of the lengths of the brightening loops as a function of the soft X-ray peak intensity through Al 1265 Å filter. It is assumed that the errors in the length are ±1 CCD pixel size (2.″46).

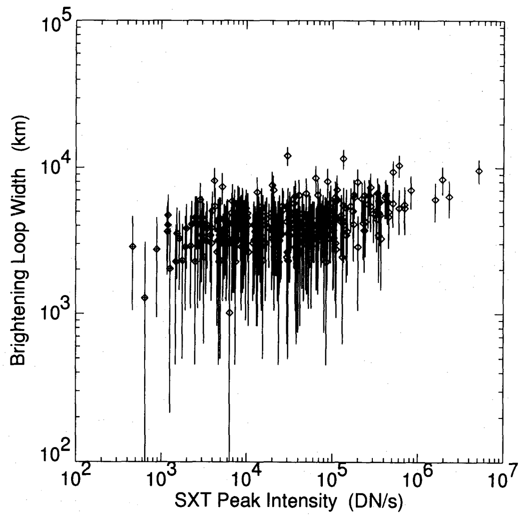

Fig. 5. Distribution of the widths of the brightening loops as a function of the soft X-ray peak intensity through Al 1265Å filter. It is assumed that the errors in the width are ±1 CCD pixel size (2.″46).

size (2.″46). The loop length ranges from 5×10^3 to 4×10^4 km. Brighter events tend to have longer loops. The width ranges from 2×10^3 to 7×10^3 km. The aspect ratio (width/length) of the brightening loops is distributed from 0.1 to 1.

The temperature and volume emission measure at the peak phase are shown in figure 6. Note that we obtained the temperature and the volume emission measure at the peak of the soft X-ray intensity. The error bars on the temperature and emission measure represent $\pm 1\sigma$ uncertainties based on Poisson statistics of the incident photons. The estimated temperatures are concentrated around 4–8 MK, whereas the emission measures are widely distributed from $10^{44.5}$ to $10^{47.5}$ cm^{-3}. A similar tendency between the temperature and emission measure has been found in GOES A-class activities by Watanabe (1993).

Major flares (GOES X and M class) are typically observed having temperatures of 8–10 MK by SXT with the same filter combination, and have the emission measures of 10^{48}–10^{51} cm^{-3} (e.g., Acton et al. 1992). Also, the Skylab soft X-ray data gives temperatures of about 10 MK and emission measures of 10^{49}–10^{50} for compact major flares (Moore et al. 1980). Transient brightenings have significantly smaller emission measures than do major flares. The temperatures of transient brightenings are also lower than those of major flares.

Assuming that the plasma depth along the line of sight is equal to the width of the brightening loops (w), the electron density (N_e) can be given by

$$N_\mathrm{e} = \sqrt{\frac{EM}{lw^2}}, \tag{3}$$

where EM is the volume emission measure and l the length of the loops. We should note that we are assuming a filling factor of unity. In figure 7, the distribution of the electron densities is shown as a function of the SXT peak intensity. The error bars on the electron density are derived using the errors in the emission measure and the loop size. The electron densities are distributed in the range of 2×10^9 to 2×10^{10} cm^{-3}. These values are one order of magnitude lower than those of the major flares ($\sim 10^{11}$ cm^{-3}) obtained with the Skylab X-ray data (Moore et al. 1980) as well as with the Yohkoh SXT X-ray data (e.g., Acton et al. 1992).

The gas pressure (p) in the brightening loops is given by

$$p = 2N_\mathrm{e}k_\mathrm{B}T, \tag{4}$$

where k_B is Boltzmann's constant. The distribution of gas pressures is shown as a function of the peak intensity in figure 8. The gas pressures are distributed from 2 to 50 dyne cm^{-2}, most of which are concentrated from 5 to 20 dyne cm^{-2}. It appears that more energetic transient brightenings have a higher gas pressure.

For confined flux tubes, such as brightening loops, the magnetic pressure should be larger than the gas pressure,

$$p < \frac{B_\mathrm{G}^2}{8\pi}, \tag{5}$$

where B_G is the magnetic-field strength in Gauss. The lower limit of B_G is 35 G for 50 dyne cm^{-2}, and 7 G for

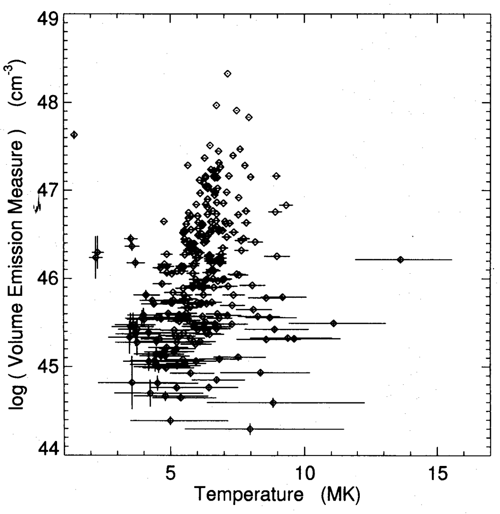

Fig. 6. Temperature and volume emission measure of the transient brightenings at the X-ray peak intensity. A combination of the peak intensities of Al 1265 Å and Al 12 μm filters is used with the assumption of soft X-ray emission from isothermal plasma. The error bars on the temperature and emission measure represent ± 1 σ uncertainties based on Poisson statistics of the incident photons.

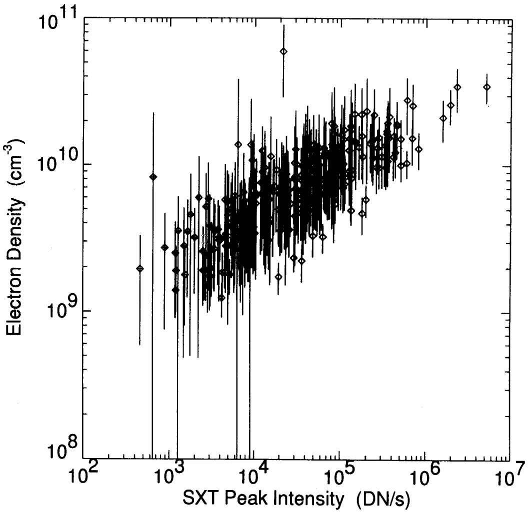

Fig. 7. Distribution of the electron densities in the brightening loops as a function of the SXT peak intensity. We assume that the plasma depth along the line of sight is equal to the width of the loops. The error bars on the electron density were derived using the errors in the emission measure and the loop size.

2 dyne cm^{-2}. The magnetic energy ($E_{\rm m}$) involved in a brightening loop can be represented by

$$E_{\rm m} = \frac{B_{\rm G}^2}{8\pi} l w^2. \quad (6)$$

Since the field strength used here is the lower-limit value, this equation gives the lower limit of the magnetic energy. Assuming 10^4 km of loop length and 5×10^3 km of loop width as typical values, 10^{28} and 5×10^{26} erg are the magnetic energy for 35 and 7 G, respectively. The magnetic energy is roughly sufficient to produce transient brightenings, the released energy of which is about 10^{25}–10^{29} erg (see the next section).

The physical parameters of the transient brightenings obtained here are summarized in table 1.

Table 1. Physical parameters of transient brightenings.

Physical parameter	Value
Temperature	4–8 MK
Volume emission measure	$10^{44.5}$–$10^{47.5}$ cm^{-3}
Electron density	2×10^9–2×10^{10} cm^{-3}
Gas pressure	5–20 dyne cm^{-2}
Loop length	5×10^3–4×10^4 km
Loop width	2×10^3–7×10^3 km
Duration	2–7 min
Total loss energy (radiation plus thermal conduction)	5×10^{26}–5×10^{29} erg
Scaled total energy loss (see text subsection 4.2)	10^{25}–10^{29} erg
Thermal energy content	10^{26}–10^{29} erg

4. Released Energy and Occurrence Rate of Transient Brightenings

4.1. Frequency Distribution of the Soft X-Ray Peak Intensity

The differential distribution of the occurrence rate of the transient brightenings obtained from the visual inspection method is shown in figure 9. The horizontal bin width is 0.2 in log (SXT peak intensity). A bin width of 0.2 is sufficiently larger at 10^4 DN s^{-1} than the photon noise ($\leq$ 100 DN s^{-1}). We could not find any significant change in the slope of the distribution when we changed the bin width from 0.05 to 0.4 in log (SXT peak intensity). The error bars on the differential distribution represent ± 1 σ uncertainties based on Poisson statistics of the number of events in each bin.

It is apparent in figure 9 that fainter transient brightenings occur more frequently than do bright events. The distribution of the peak intensity of the transient brightenings can be well represented by a flat power-law over 2 orders of magnitude within ± 2 σ uncertainties. The turn-over in the distribution at the lower end of magnitude probably results from the instrument dead time

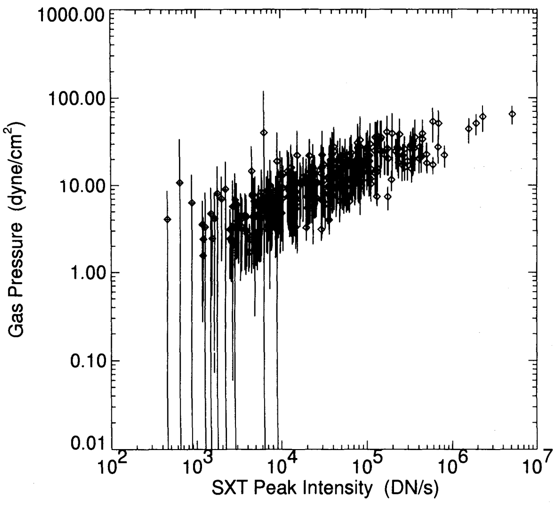

Fig. 8. Distribution of the gas pressures in the brightening loops as a function of the SXT peak intensity. The error bars on the gas pressure were derived using the errors in the temperature and the electron density.

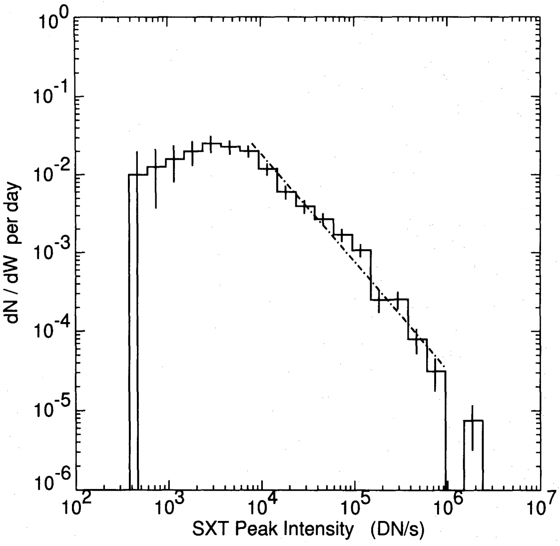

Fig. 9. Frequency distribution of the transient brightenings as a function of the soft X-ray peak intensity. The horizontal axis is the soft X-ray peak intensity of the transient brightenings above the background through Al 1265 Å filter. The total number of the transient brightenings used in this study was 291. The error bars represent $\pm 1\sigma$ uncertainties based on Poisson statistics of the number of events in each bin. The distribution can be fitted by a power-law with index 1.4 (dash-dotted line) in the range of 8×10^3 to 10^6 DN s^{-1}.

and/or the reduced efficiency of finding faint events obscured by bright background. The typical exposure time is 338 ms for the Al 1265 Å filter data and 5.3 s for the Al 12 μm filter data, and the exposure interval is 32 s. The duty cycle is only 9%, biasing the search against faint short-lived events. The slope of the least-squares power-law is found to be 1.4 ± 0.1 for 9×10^3 through 10^6 DN s^{-1}.

One of the main disadvantages in the visual-inspection method may be to miss some faint brightenings appearing in the bright diffuse background of the active region. This effect contributes to the roll-over at the lower end of energy range, as shown in figure 9. We developed the macro-pixel method in order to systematically find X-ray intensity enhancements for studying the significance of this effect. Details concerning the method are described in section 2. The distribution derived by the macro-pixel method is shown in figure 10. Figure 10a gives the distribution derived from a macro-pixel size of 8×8 pixels and figure 10b is that from a macro-pixel size of 16×16 pixels. These figures show that the distributions are well fitted with a flat power-law. The power-law dependence is more evident in the macro-pixel method than in the visual inspection method. The power-law distribution continues at least down to 5×10^3 DN s^{-1}, which is a factor of 5 smaller than the location of the turn-over in the visual inspection method.

The dependence of power-law index on the macro-pixel size is summarized in table 2. The loop size of the transient brightenings is observed to be about 3–16 CCD pixels (figures 4 and 5); we thus varied the macro-pixel size from 4 to 20 pixels. Since one transient brightening can split into a few macro-pixels, we have made a correction, as described in section 2. The power-law index has values of 1.63–1.89, depending on the macro-pixel size. This dependence is caused by two effects: (1) it is more sensitive to detect smaller-scaled fainter enhancements in smaller macro-pixel cases, and (2) the event-splitting effect is less perfectly corrected by the macro-pixel method in smaller macro-pixel cases. This result, however, shows that the power-law index of the frequency distribution of transient brightenings is smaller than 2.

The power-law index obtained with the visual-inspection method is 1.4, whereas the index obtained by the macro-pixel method is among 1.63–1.89. There is a discrepancy between these values. Does the visual inspection method miss a large number of faint transient brightenings which appear in the bright diffuse backgrounds of the active region? We find that the light curves of the macro-pixel intensities have many tiny enhancements which are not detectable by a visual inspection. These enhancements may make the power-law index increase. The nature of these events will be described in a separate paper.

The macro-pixel method clearly shows that the occur-

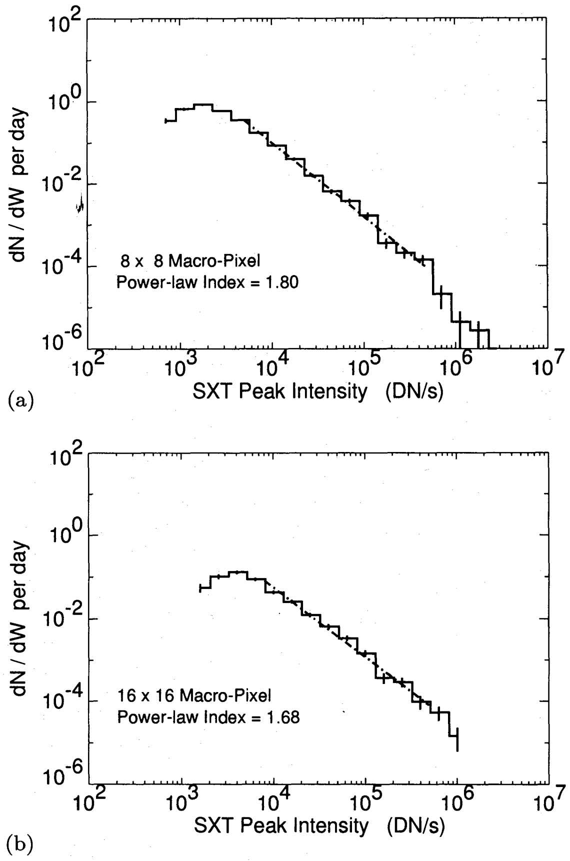

Fig. 10. Distribution of the peak intensity derived by the macro-pixel method with the macro-pixel sizes of (a) 8×8 pixels and (b) 16×16 pixels. The horizontal axis is the soft X-ray peak intensity in the excess of the background. The error bars represent $\pm 1\ \sigma$ uncertainties based on Poisson statistics of the number of events in each bin. The power-law distribution continues downward to less than 10^4 DN s^{-1}. The differences in the power-law index and the total event number are probably due to the event-splitting effect discussed in the text.

rence rate of the transient brightenings has a power-law dependence down to the lowest limit of the SXT sensitivity, although it does not yield an accurate power-law index of the distribution at the low end, due to the slightly imperfect correction of the event-splitting effect. However, we can conclude that the power-law index of the frequency distribution of transient brightenings is smaller than 2.

4.2. Energy Estimation

In order to examine whether the transient brightenings can contribute to heating of active-region corona, we estimate the total energy released by the transient brightenings into the active-region corona. The total released energy is estimated using two independent calculations: (1) the total loss energy (radiation plus thermal conduction) and (2) the scaled total energy loss by applying the empirical conversion formula described in Hudson(1991). In addition, we obtain the thermal energy content of the brightening loops. The accuracy of the energy estimation used in this study is discussed in appendix 2.

4.2.1. Total loss energy

The total loss energy is the sum of the radiative and conductive losses of the hot plasma in the brightening loops. A considerable amount of energy in the hot plasma is transported by thermal conduction and radiation (e.g., Priest 1982; Machado 1991). The generation of a hot plasma in the corona may set up a strong temperature gradient; energy is then transported along a coronal loop into the cool chromosphere. Furthermore, the hot plasma radiates soft X-rays through thermal bremsstrahlung, and energy is transported radiatively towards the heliosphere as well as downwards into the transition region, chromosphere, and upper photosphere. In energy transport, although mass motions may also play a role, we ignore here energy transport by mass motions.

The radiative loss ($F_{\rm r}$) can be calculated using

$$F_{\rm r} = N_{\rm e}^2\, P(T)\, V, \tag{7}$$

where $N_{\rm e}$ is the electron density and $P(T)$ the radiative loss function of a plasma of temperature T from Raymond, Cox, and Smith (1976) with an analytic fit of Rosner, Tucker, and Vaiana (1978). The plasma volume V is simply assumed to be equal to lw^2 here. The filling factor of the hot plasma is assumed to be unity. The conductive loss ($F_{\rm c}$) is

$$\begin{aligned} F_{\rm c} &= \kappa T^{5/2} \nabla T A \\ &= 2\kappa T^{7/2} \frac{w^2}{l}, \end{aligned} \tag{8}$$

(Spitzer 1962), where κ is the classical Spitzer coefficient (1.1×10^{-6} erg cm^{-3} s^{-1} K$^{7/2}$) and A is the cross section of a coronal loop (w^2). Since thermal conduction across the field lines is greatly suppressed in the coronal loops, the temperature gradient can be approximately written as $\nabla T \ = \ 2T/l$, where we use $l/2$ as the temperature-variation scale length. Thus, the total loss energy ($E_{\rm loss}$) is defined as

$$E_{\rm loss} \ = \ (F_{\rm r} + F_{\rm c})\, t_{\rm D}, \tag{9}$$

where $t_{\rm D}$ is the observed duration of the transient brightenings.

4.2.2. Scaled total energy loss

Hudson (1991) developed empirical conversion formulae to obtain the frequency distributions of the total flare energy. Based on these conversions, he presented a plot describing the distributions of the total flare energy for

Table 2. Dependence of power-law index on macro-pixel size.

Macro pixel size (pixels)	Power-law index	Fitting range (DN s^{-1})	Total number (all)	Event number (> 10^4 DN s^{-1})
4 × 4	1.89	5×10^3–5×10^5	5008	651
6 × 6	1.86	5×10^3–5×10^5	2992	582
8 × 8	1.80	5×10^3–5×10^5	2041	562
10 × 10	1.77	5×10^3–5×10^5	1302	473
12 × 12	1.78	5×10^3–5×10^5	967	415
14 × 14	1.63	5×10^3–7×10^5	851	419
16 × 16	1.68	8×10^3–5×10^5	706	352
18 × 18	1.67	8×10^3–5×10^5	552	313
20 × 20	1.64	8×10^3–1×10^6	376	226

different sets of X-ray observations of solar flares, including hard X-ray microflares. The conversions are based upon the empirical hypothesis that the peak soft X-ray radiation flux measures the total radiant energy release in a solar flare according to the luminosity ratio,

$$L_{\rm SXR}/L_{\rm total} = 2/30. \qquad (10)$$

[Note that Hudson (1991) has a misprint in the formula and the luminosity ratio given here is correct (Hudson 1993 private communication).] This estimate is an order-of-magnitude estimate, because we have little knowledge concerning the radiation flux as a function of the wavelength. We should note that this ratio is based on the observations of several large flares (Wu et al. 1986).

The total soft X-ray luminosity (energy) is estimated by multiplying the radiative loss by the observed duration. Thus, the scaled total energy loss ($E_{\rm scaled}$) is given by

$$E_{\rm scaled} = \frac{30}{2} F_{\rm r}\, t_{\rm D}. \qquad (11)$$

4.2.3. Thermal energy content

The thermal energy content ($E_{\rm th}$) of the hot plasma in a brightening loop is

$$E_{\rm th} = 3\, N_{\rm e}\, k_{\rm B}\, T\, V. \qquad (12)$$

The filling factor of the plasma is assumed to be unity.

4.3. Distributions of the Occurrence Rate as a Function of Energy

Frequency distributions of the transient brightenings are shown in figure 11 as a function of the total energy described in the previous section. The dotted line represents the total loss energy (radiation plus thermal conduction), the dashed line the scaled total energy loss, and the solid line the thermal energy content, respectively.

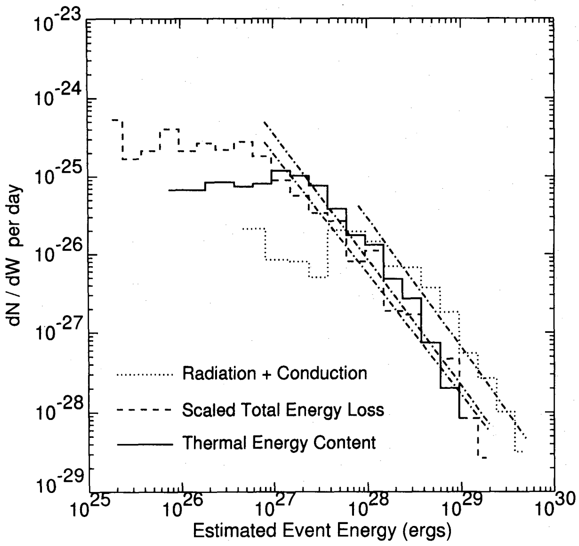

Fig. 11. Frequency distribution of the transient brightenings as a function of the total energy: radiation plus conduction loss (dotted line), scaled total energy loss (dashed line), and thermal energy content (solid line). Each distribution can be represented by a single power-law with the index 1.5–1.6 (dash-dotted lines), although the distribution deviates from the power-law at the lower end of energy range.

Each distribution can be represented by a single flat power-law with an index of 1.5–1.6 in the energy range of 10^{27} through 10^{29} erg, although the distribution deviates from the power-law at the lower end of the energy range (smaller than 10^{27} erg). This index is smaller than that of the distribution of hard X-ray microflares (Lin et al. 1984) as well as that of the distribution of the hard X-ray peak count of major flares (1.7–1.8, e.g., Dennis 1985). It is, however, in good agreement with that of the distribution of the total flare energy of major flares with the thick-target calculation (1.53, Crosby et al. 1993).

We should note that the transient brightenings observed by SXT are distributed from 10^{25} to 10^{29} erg, whereas Lin et al.'s microflares are from 10^{27} to 10^{28} erg. This implies that the transient brightenings are at or below the range of the hard X-ray microflares. Considering the distribution of major flares in addition to that of the transient brightenings, the power-law distribution continues with the same slope of 1.5–1.6 from an energy of 10^{32} erg down to $< 10^{27}$ erg over a range of more than five orders of magnitude. No significant increase in the slope of the frequency distribution is found in the energy range of the transient brightenings.

The total energy estimated here can be summarized as follows (see also table 1): the energy range of the total loss energy (radiation plus thermal conduction) is from 5×10^{26} to 5×10^{29} erg, the scaled total energy loss from 10^{25} to 10^{29} erg, and the thermal energy content from 10^{26} to 10^{29} erg. The estimation of the total loss energy (radiation plus thermal conduction) provides slightly larger values than does the other estimation. This discrepancy may result from uncertainty in the quantities and the assumptions used to derive the energetics terms. The accuracy of the energy estimation is discussed in appendix 2.

5. Energy Input by Transient Brightenings

Here, we give a rough estimation of the energy input due to transient brightenings and flares. The energy input of the sum of transient brightenings can be easily estimated using figure 11. Here, we adopt a power-law distribution of the total loss energy (radiation plus thermal conduction), which will give a relatively larger value than the other distribution, as an exercise, and assume that this distribution continues from 10^{32} erg downward to the nanoflare energy ($< 10^{24}$ erg) range. The estimated energy input by transient brightenings end flares is 2.7×10^{27} erg s^{-1}.

To compare this energy input with the energy input required for the heating of an active region, we estimate the radiative and conductive losses in the active region NOAA 7260. We find the temperature of this active region to be 5.7 MK, and the column emission measure 1.5×10^{28} cm^{-5} on the average. Assuming the line-of-sight thickness to be the diameter of the active region, the electron density can be derived to be 9.9×10^{8} cm^{-3}. The radiative loss rate is then estimated to be 2.1×10^{26} erg s^{-1} and the conductive loss rate is 1.4×10^{28} erg s^{-1}. The energy input into this active region should be roughly 1.5×10^{28} erg s^{-1}. Note that the energy input obtained here is slightly larger than the usually accepted value shown in Withbroe and Noyes (1977).

Therefore, the total energy supplied by the sum of transient brightenings and flares is about a factor of 5 smaller than the energy input required for heating of the active-region corona.

6. Summary and Discussions

6.1. *Summary of Observation*

In this paper we have described the distribution of the occurrence rate of transient brightenings. We also estimated the physical parameters of the brightening loops at the soft X-ray peak phase (table 1).

This study shows that the distribution of the occurrence rate of transient brightenings versus the soft X-ray peak intensity can be represented by a flat power-law. The power-law index is 1.4 ± 0.1 from the visual-inspection method and between 1.63 and 1.89 based on the macro-pixel method. We also estimated the total energy released by the transient brightenings, and, thus, the frequency distribution of the transient brightenings as a function of energy. The total released energy was estimated by two independent calculations (radiation plus thermal conduction, and the scaled total energy loss). The thermal energy content was also obtained. These estimations provide a single power-law as a function of energy with an index of 1.5–1.6 in the energy range of 10^{27}–10^{29} erg. The index of 1.5–1.6 can be compared with the power-law index of 1.53 of the distribution of the total flare energy of major flares calculated by integrating the thick-target energy rate over the hard X-ray flare duration (Crosby et al. 1993). This means that the power-law index of the transient brightenings is in good agreement with that of major flares, and that a single power-law distribution continues from 10^{32} erg downward to less than 10^{27} erg.

6.2. *Implications for Coronal Heating*

We now discuss whether the transient brightenings can contribute to the heating of the active-region corona. The present study shows a single power-law distribution of the occurrence rate of transient brightenings with an index smaller than 2. No apparent increase in the power-law index is observed as we go to fainter events. The estimation of the energy input also shows that the total energy released by the sum of transient brightenings and flares is at most a factor of 5 smaller than the heating rate required for the active-region corona in the case of the active region NOAA 7260.

There is, however, still the possibility that the transient brightenings may contribute substantially to coronal heating. First, we have not obtained an accurate frequency distribution in the energy range smaller than 10^{27} erg. We need to find weaker events ($< 10^{27}$ erg) with an occurrence rate much higher than the extrapolated power-law to explain the heating of active regions with transient brightenings. Second, UV microflares, which are numerous tiny enhancements observed in C IV line (Porter et al. 1984), are observed more frequently than the hard X-ray microflares (Porter et al. 1995). This may imply that smaller energy releases are produced much more in a low-temperature plasma than in a high-temperature plasma. If this is the case, the transient brightenings observed in the soft X-ray wavelengths are only a part of all the small energy releases. Third, energetics terms, which were ignored in this study, such as plasma flows, may make additional contributions to the energy input. Some transient brightenings appear near the roots of high, long loops. The enhanced coronal heating in these high loops is observed to be associated with the transient brightenings (Porter et al. 1994). Moreover, coronal X-ray jets, which are transient X-ray enhancements with an apparent collimated motion, are observed to be associated with small flares (Shibata et al. 1992). The kinetic energy of the jets is on the order of 10^{26}–10^{28} erg, although the jets are usually very faint features (Shibata et al. 1994). If the transient brightenings have a component of invisible jet-like features, the total energy of the transient brightenings would be larger than the total energy estimated in this study. It is also found that the global expansions of active regions may be the result of occurrences of the transient brightenings (Uchida et al. 1992). Energy may not be transported from the brightenings to the expansions, but the brightenings may trigger other global energy releases.

Transient brightenings appear mainly in confined compact loops, whereas active regions consist largely of diffuse steady loops (Kano, Tsuneta 1994). The largest amount of soft X-ray emission comes from steady loops. If the transient brightenings contribute to the heating of the active-region corona, a large amount of energy should be transported from the transient brightenings into steady loops. Since thermal conduction across magnetic field lines is greatly suppressed in the coronal loops, magnetosonic waves which can propagate across the magnetic-field lines and the plasma flow described above may transfer energy to outside the transient brightenings. Another possibility to explain the steady loops is that the steady loops are heated by numerous nanoflares (Parker 1988), which would be energetically smaller than transient brightenings. Since these nanoflares are small-scale, tiny energy releases, they may show no enhancements in X-ray brightness (Kopp, Poletto 1994; Cargill 1994).

6.3. Power-Law Distribution

This paper has shown that a single power-law distribution continues downward to at least 10^{27} erg. The frequency distribution of solar flares including transient brightenings can be represented by a single power-law over more than five orders of magnitude in total energy. This broad distribution should be explained from the viewpoint of an unified understanding of coronal energy releases. Several theoretical models have been developed to explain this broad power-law behavior. Rosner and Vaiana (1978) propose a model in which the energy releases are a stochastic relaxation phenomenon. Lu and Hamilton (1991) propose a new idea in which this distribution can be understood as avalanches of many small events. This idea predicts that the power-law index of the frequency distribution would be independent of solar activity, and the same in different active regions (Lu et al. 1993). We need to investigate the possible activity dependence (cf. Bai 1993) or active-region dependence by using the Yohkoh soft X-ray data.

The author would like to express his thanks to all the Yohkoh team members for the instrument development and daily operation. He would like to thank Dr. S. Tsuneta for suggesting the topics presented in this paper and kindly reading this manuscript with many helpful comments. He also thank Drs H. Hudson, M. Bruner, J. Lemen, L. Acton, T. Watanabe, T. Sakurai, and Y. Uchida for helpful comments. This work was carried out while the author held a Fellowship from the Japan Society for the Promotion of Science for Young Scientists.

Appendix 1. SXT Intensity versus GOES Intensity

As discussed in Shimizu et al. (1992), intense transient brightenings can be observed as small enhancements in the GOES time profiles, when the X-ray quiescent level is low. The relation between the SXT and GOES intensities of transient brightenings is shown in figure 12. The SXT intensity is the peak intensity in excess of the background, while the GOES intensity is the maximum intensity of the corresponding enhancements, which is measured without subtracting any quiescent components. The GOES measurement in the high channel (0.5–4 Å) is used in this plot, because we can observe the small enhancements in the high channel more frequently than in the low channel (1–8 Å). The SXT and GOES intensities have a linear dependence in log-log space (the dash-dotted line is a least-squares fit): 6×10^6 and 2×10^5 DN s^{-1} in the SXT intensity correspond to 10^{-7} and 2×10^{-9} W m^{-2} in the GOES intensity, respectively. For some transient brightenings, we measure the GOES intensity in the low channel. The transient brightenings with an intensity of 10^7 DN s^{-1} are observed to roughly correspond to C1 class activities and 10^6 DN s^{-1} to B5 class activities. Note that we can observe transient brightenings as faint as 10^3 DN s^{-1}. These faint brightenings are generally not detectable in the GOES high-channel data. They may, however, be observed in

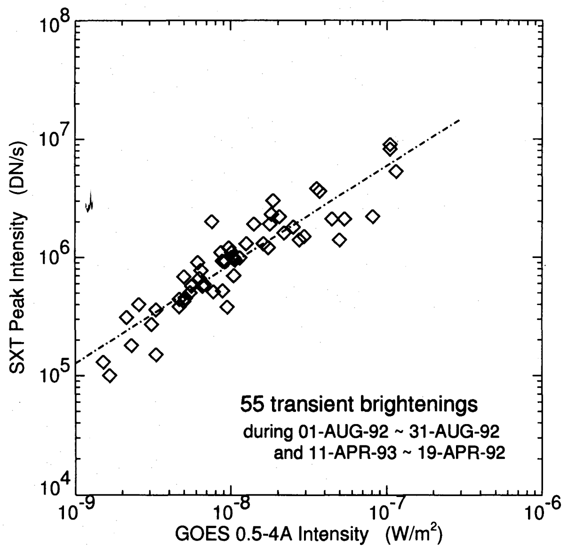

Fig. 12. Soft X-ray intensity of intense transient brightenings measured by SXT and GOES. The vertical axis is the soft X-ray peak intensity of the transient brightenings in the excess of the background intensity which is measured at the SXT focal plane through Al 1265 Å filter, and the horizontal axis is the maximum intensity of the corresponding enhancements (no subtraction of the quiescent background intensity) which is measured in the GOES high channel (0.5–4 Å). Note that SXT can observe transient brightenings as faint as 10^3 DN s^{-1}, which are not detectable in the GOES data.

the low channel if the X-ray quiescent level is in the low end of A class.

Appendix 2. Accuracy of Energy Estimation

Here, we discuss the accuracy of the energy estimation used in this study.

The conversion formula used to estimate the scaled total energy loss may not be sufficiently accurate. Several attempts have been made to obtain a representative luminosity ratio for major flares (e.g., Thomas, Teske 1971; Lin, Hudson 1976; Canfield et al. 1980). These suggest that the soft X-ray radiation is about 5–15% of the total flare energy. Their luminosity ratios are approximately in agreement with the ratio used in this study [equation (10)], although they have a relatively large deviation.

In estimating the total loss energy, the heat-conduction flux along cylindrical coronal loops is applied using classical Spitzer theory. The magnetic fields that fill the brightening loops may, however, be rooted in a small fraction of the solar surface. The convergence of the coronal loops may significantly reduce the heat conduction from the corona (e.g., Antiochos, Sturrock 1976; Dowdy, Moore, and Wu 1985). In addition, we ignore the response of the chromosphere and transition region to the heat conduction (Hirayama 1974) as well as the mass flows (chromospheric evaporation) in the loops caused by heat conduction (e.g., Antiochos, Sturrock 1978; Fisher, Hawley 1990). Note that we observe initial brightenings from the loop footpoints for some transient brightenings (Shimizu et al. 1994).

Another uncertainty in the energy estimation is that of the filling factors. Here, we have assumed a filling factor of unity. If, for example, the filling factor is 0.01, the electron density would be increased by an order of magnitude. This effect in the energy estimation is to reduce the thermal energy content by an order of magnitude, and the conductive loss by two orders of magnitude, although it does not affect the estimation of the radiative loss. Here, we simply assume that any fine structure giving rise to a small filling factor comprises long, thin strands which still communicate to the lower chromosphere.

We estimate the timescales of the radiative and conductive losses for typical transient brightenings, to compare with the observed duration. Representative values of the physical parameters are used here: the plasma temperature is 7 MK; electron density, 8×10^9 cm^{-3}; loop length, 1.8×10^4 km; and loop width, 4.5×10^3 km. Thermal energy content is 8.5×10^{27} erg. The radiative loss from the brightening loop is 1.2×10^{24} erg s^{-1} and its cooling timescale is 7×10^3 s, whereas the conductive loss is 2.2×10^{26} erg s^{-1} and its cooling timescale is 40 s. These timescales mean that the brightening loops are more effectively cooled by heat conduction rather than by radiation. We should note that the typical observed duration of the transient brightenings is 250 s (figure 3). This is much longer than the conductive cooling timescale, whereas it is shorter than the radiative cooling timescale. The difference between the duration and the conductive cooling timescale is so significant that it may imply continuous heating. However, this conclusion is not solid, because of the uncertainties discussed above. The small filling factor reduces the radiative cooling time by an order of magnitude and increases the conductive cooling time by the same order. If, for example, the filling factor is 0.01, the radiative cooling time would be reduced to 700 s, and the conductive cooling time would be increased to 400 s. Since these timescales are longer than the typical observed duration of the transient brightenings, the transient brightenings do not need continuous heating.

References

Acton L.W., Feldman U., Bruner M.E., Doschek G.A., Hirayama T., Hudson H.S., Lemen J.R., Ogawara Y. et al. 1992, PASJ 44, L71

Antiochos S.K., Sturrock P.A. 1976, Solar Phys. 49, 359

Antiochos S.K., Sturrock P.A. 1978, ApJ 220, 1137
Bai T. 1993, ApJ 404, 805
Canfield R.C., Cheng C.-C., Dere K.P., Dulk G.A., McLean D.J., Robinson R.D. Jr, Schmahl E.J., Schoolman S.A. 1980, in Solar Flares (A Monograph from Skylab Solar Workshop II) ed P.A. Sturrock (Colorado Associated University Press, Boulder) p451
Cargill P.J. 1994, ApJ 422, 381
Crosby N.B., Aschwanden M.J., Dennis B.R. 1993, Solar Phys. 143, 275
Datlowe D.W., Elcan M.J., Hudson H.S. 1974, Solar Phys. 39, 155
Dennis B.R. 1985, Solar Phys. 100, 465
Dowdy J.F. Jr, Moore R.L., Wu S.T. 1985, Solar Phys. 99, 79
Drake J.F. 1971, Solar Phys. 16, 152
Fisher G.H., Hawley S.L. 1990, ApJ 357, 243
Hara H., Tsuneta S., Lemen J.R., Acton L.W., McTiernan J.M. 1992, PASJ 44, L135
Harvey K., Harvey J. 1973, Solar Phys. 28, 61
Hirayama T. 1974, Solar Phys. 34, 323
Hudson H.S. 1991, Solar Phys. 133, 357
Kano R., Tsuneta S. 1994, ApJ submitted
Kopp R.A., Poletto G. 1993, ApJ 418, 496
Lee T.T., Petrosian V., McTiernan J.M. 1993, ApJ 412, 401
Leka K.D., van Driel-Gesztelyi L., Nitta N., Canfield R.C., Mickey D.L., Sakurai T., Ichimoto K. 1994, Solar Phys. 155, 301
Lin R.P., Hudson H.S. 1976, Solar Phys. 50, 153
Lin R.P., Schwartz R.A., Kane S.R., Pelling R.M., Hurley K.C. 1984, ApJ 283, 421
Lu E.T., Hamilton R.J. 1991, ApJL 380, L89
Lu E.T., Hamilton R.J., McTiernan J.M., Bromund K.R. 1993, ApJ 412, 841
Machado M.E. 1991, Phil. Trans. R. Soc. Lond. A 336, 425
Moore R., McKenzie D.L., Švestka Z., Widing K.G., Antiochos S.K., Dere K.P., Dodson-Prince H.W., Hiei E. et al. 1980, in Solar Flares (Monograph from Skylab Solar Workshop II), ed P.A. Sturrock (Colorado Associated University Press, Boulder) p341
Ogawara Y., Takano T., Kato T., Kosugi T., Tsuneta S., Watanabe T., Kondo I., Uchida Y. 1991, Solar Phys. 136, 1
Parker E.N. 1988, ApJ 330, 474
Porter J.G., Fontnela J.M., Simnett G.M. 1995, ApJ 438, 472
Porter J.G., Moore R.T., Roumeliotis G., Shimizu T., Tsuneta S., Sturrock A., Acton L.W. 1994, in Proceedings of Kofu Symposium (NRO No.360) ed S. Enome, T. Hirayama (Nobeyama Radio Observatory, NAOJ, Nobeyama) p65
Porter J.G., Toomre J., Gebbie K.B. 1984, ApJ 283, 879
Priest E.R. 1982, Solar Magnetohydrodynamics (Reidel, Dordrecht) p82
Raymond J.C., Cox D.P., Smith B.W. 1976, ApJ 204, 290
Rosner R., Tucker W.H., Vaiana G.S. 1978, ApJ 220, 643
Rosner R., Vaiana G.S. 1978, ApJ 222, 1104
Shibata K., Ishido Y., Acton L.W., Strong K.T., Hirayama T., Uchida Y., McAllister A.H., Matsumoto R. et al. 1992, PASJ 44, L173
Shibata K., Yokoyama T., Shimojo M. 1994, in Proceedings of Kofu Symposium (NRO No.360) ed S. Enome, T. Hirayama (Nobeyama Radio Observatory, NAOJ, Nobeyama) p75
Shimizu T. 1993, in Proceedings of the 2nd Japan-China Seminar on Solar Physics, ed T. Sakurai, T. Hirayama, G. Ai (National Astronomical Observatory of Japan, Tokyo) p193
Shimizu T. 1994, in X-Ray Solar Physics from Yohkoh, ed Y. Uchida, T. Watanabe, K. Shibata, H.S. Hudson (Universal Academy Press, Tokyo) p33
Shimizu T., Tsuneta S., Acton L.W., Lemen J.R., Ogawara Y., Uchida Y. 1994, ApJ 422, 906
Shimizu T., Tsuneta S., Acton L.W., Lemen J.R., Uchida Y. 1992, PASJ 44, L147
Spitzer L. 1962, Physics of Fully Ionized Gases (Interscience, New York) p122
Thomas R.J., Teske R.G. 1971, Solar Phys. 16, 431
Tsuneta S., Acton L., Bruner M., Lemen J., Brown W., Caravalho R., Catura R., Freeland S. et al. 1991, Solar Phys. 136, 37
Tsuneta S., Lemen J.R. 1993, in Advances in Stellar and Solar Coronal Physics, ed J.F. Linsky, S. Serio (Kluwer, Dordrecht) p113
Uchida Y., McAllister A., Strong K.T., Ogawara Y., Shimizu T., Matsumoto R., Hudson H.S. 1992, PASJ 44, L155
Vaiana G.S., Krieger A.S., Timothy A.F. 1973, Solar Phys. 32, 81
Watanabe Te. 1993, in Proceedings of Kofu Symposium (NRO No.360), ed S. Enome, T. Hirayama (Nobeyama Radio Observatory, NAOJ, Nobeyama) p99
Withbroe G.L., Noyes R.W. 1977, ARA&A 15, 363
Wu S.T., de Jager C., Dennis B.R., Hudson H.S., Simnett G.M., Strong K.T., Bentley R.D., Bornmann P.L. et al. 1986, in Energetic Phenomena on the Sun, ed M. Kundu, B. Woodgate (NASA CP-2439) p5-1